17 (2023) 100301

Contents lists available at ScienceDirect

International Journal of Thermofluids

journal homepage: www.sciencedirect.com/journal/international-journal-of-thermofluids

CFD analyses for the development of an innovative latent thermal energy storage for food transportation

Michele Calati [a], Giulia Righetti [a], Claudio Zilio [a], Kamel Hooman [b], Simone Mancin [a,*]

[a] Department of Management and Engineering, University of Padova, S.lla San Nicola, 3, Vicenza 36100, Italy
[b] Department of Process and Energy, Delft University of Technology, Delft, the Netherlands

ARTICLE INFO

Keywords:
Phase change material
Cold chain
Energy management
Food Transportation

ABSTRACT

The transportation of perishable products is a crucial activity that must be carefully managed along the cold chain. The refrigerated transport aims at ensuring the suitable transportation conditions by maintaining the desired temperature level in the refrigerated compartment. Moreover, the carriage of perishable fresh foodstuffs calls for additional precautions due to the intrinsic metabolic activity of fresh foods which causes them to be highly temperature sensitive. About 30% of fresh products perishes on the route due to the loss of suitable temperature values. Recently, scientists have been focusing their efforts on the development of innovative solutions, which ensure a proper refrigerated products distribution and transportation in a more environmental-friendly and cost-effective way. Hence, in this work, a novel concept of a Latent Thermal Energy Storage (LTES) system consisting of an insulation layer of poly-urethane foam wrapping a second one of Phase Change Material (PCM) is proposed. In particular, the thermal performance is investigated by running numerical CFD analyses in Ansys Fluent. The effect of different product loads (25%-50%-75%) is studied. Besides, the contributions of the heat respiration and diverse food pre-cooling temperatures on the system performance are also analysed. For the long-distance route no door openings nor additional heat infiltrations are considered.

1. Introduction

The cold chain consists of different main stages which can be listed in food harvesting, preconditioning, transport, bulk storage, retail, domestic and food service [1]. Due to the lack of the optimal temperature conditions, food wastages and losses occur. It has been estimated that more than 1 billion ton of produced food is lost or wasted every year [2] having, not only social and environmental, but also financial consequences. In fact, the food wastages and losses result in a $940 billion financial loss [3]. The great amount of perished food is in contrast with the "Zero Hunger" program, which is one the seventeen 2030 Sustainable Development Goals (SDGs) established by the United Nations [4] to fight and reduce the huge number of 820 million people malnourished worldwide [5]. In addition to the social and financial aspects, the environmental one cannot be neglected. It has been evaluated in 4.4 Gton $CO_{2,eq}$ per year the amount of the emissions due to food wastages and losses. Moreover, it must be taken into consideration that along the cold chain, refrigeration systems based on high-GWP (Global Warming Potential) are usually employed, which account for 2.5% global greenhouse gas (GHG) emissions for both direct and indirect effects [6]. In the European Union (EU), the European Commission strongly encourages the different countries to cut down the GHG emissions due to refrigeration at least of 40% by the end of this decade [7]. A complete review of innovative technologies for applications in the food refrigeration field was assessed by Tassou et al. [8]. They may be resumed in sorption refrigeration-adsorption systems, ejector refrigeration systems, air cycle refrigeration, tri-generation, Stirling cycle refrigeration, thermoacoustic refrigeration, magnetic refrigeration, and thermoelectric refrigeration [8]. This latter exploits the Peltier effect. Two different conducting materials are joint together by the Peltier effect when a direct electric current flows through the junction and, based on the current direction, the materials are either cooled down or heated up. The thermoelectric modules are produced and sold in different sizes, going from maximum cooling capacity of less than 1 W to 310 W. Their thicknesses never overcome 5 mm. Different applications in the refrigerated sector, covering different stages of the cold chain, can be found [9]. Caglar et al. [10] investigated a portable mini thermoelectric refrigerator for drinks, fresh and cool foods, and drugs, based on a Peltier element combined with fans on both sides. It was found that the maximum COP value achieved was 0.351 after 3 min from the start of the experiment when

* Corresponding author.
E-mail address: simone.mancin@unipd.it (S. Mancin).

https://doi.org/10.1016/j.ijft.2023.100301
Received 5 December 2022; Received in revised form 1 February 2023; Accepted 1 February 2023
Available online 3 February 2023

the air temperature inside the refrigerator was 293 K. It was also obtained that the COP dropped to 0.011 when the temperature reached 255 K. Soylemez et al. [11] analyzed the cooling performance of a domestic refrigerator with thermoelectric cooling system. In particular, by means of CFD numerical analyses, the authors investigated the cooling time of the apparatus. A cooling time of 2.44 h was obtained. This value was lower than the results for the traditional commercial solutions. It was also verified that the temperature of the products closer to the thermoelectric cooler dropped below 10 °C in 2 h, suggesting that the high temperature sensitive foodstuffs should be stored at the uppermost shelf. Focusing on the refrigerated transport sector, Yuan et al. [12] studied a small insulated van based on thermoelectric cooling. The considered van presented two different zones at different target temperatures: a cold and a hot zone, with cold or hot cargo. In the wall separating the two zones, the thermoelectric cooling system was mounted. It was found that the presence of the thermoelectric cooling system could help in reducing the temperature fluctuations. In particular, in the cold zone the temperature variation dropped by 74% (from 5.8 K to 1.5 K) while in the hot zone a reduction of 13% was calculated (from 2.3 K to 2 K). Therefore, the authors [12] stated that this solution can be suitable for high temperature sensitive cargoes. Moreover, they verified that this system was indicated for short distance distribution, when a difference of 50 K between cold and hot zones can be obtained with a cold temperature ranging between 280 K and 300 K.

From what briefly reviewed, it is clear that the food refrigeration appliances based on thermoelectric cooling are still less efficient than their correspondent vapor compression technology, since their very low COP. On the contrary, the thermoelectric cooling modules do not use any moving parts, suggesting high reliability and maintenance free [8]. However, their limitations still overcome their potential advantages. In particular, as declared by Tassou et al. [13], focusing on the refrigerated transport sector, even if being more environmental friendly, the thermoelectric systems cannot compete with the traditional solutions in terms of cooling performance due to high temperature differences needed between cold and hot sides of the module, and very low COPs, where COP is obtained as the ratio between the net heat absorbed at the cold end and the electrical power applied.

In the recent years, Latent Thermal Energy Storage (LTES) systems have started to be deeply investigated as a new solution for refrigerating appliances. LTES have already found applications in different fields as solar domestic hot water systems [14] or building sector [15,16] or thermal management for electronic appliances [17]. In particular, for what concerns the cold chain, LTESs have found implementation in different applications such as refrigerating appliances [18], display cabinets [19], cold chambers [20], and refrigerated transport [21]. The main aim of a LTES is to reduce the energy consumption, ensuring contemporary an adequate temperature condition for the foodstuffs, preserving the quality and freshness and, consequently, avoiding food wastages and losses. The LTES, being a storage energy technology, let to reach the goals proposed in the EU's "20–20–20″ program and in the EC's "Energy Roadmap 2050″, as declared by Jouhara et al. [22]. This innovative solution takes advantage of the high energy density stored during the phase change process from liquid to solid (or, reversely) at an almost constant temperature by means of a Phase Change Material (PCM) [23,24]. In this way, focusing on cooling, the cold energy can be stored and used later. An ideal PCM should present an appropriate phase change temperature (depending on the application it is destined to), high thermal conductivity, and latent heat. It should experiment low volume expansion, in order to avoid PCM leakage, and it should have high density aiming at limiting the system size [25]. When dealing with food, the PCM must be no toxic and compatible with the construction materials. Promising results coming from the adoption of LTES in refrigerating appliances along the cold chain have been obtained as reviewed by Selvnes et al. [26]. Considering the cold chain, a critical stage is represented by the refrigerated transport: in fact, it plays a role from the very first phases up to the final ones. An exhaustive review covering the spread of PCM based LTESs in the refrigerated transport sector along the cold chain has been proposed by Calati et al. [27], recently. From a financial perspective, the transportation of goods has a retail value of $1200 billion [28], and it has been forecast a road cargo transport growth of 2.5% by the future ten years. Moreover, nowadays, there are 4 million refrigerated vehicles of different sizes and 1.2 million of reefers [4]. Additionally, they usually adopt low efficiency mechanical vapor compression equipment [28] having COP ranging from 0.5 to 1.5 [13]. Considering that 40% of the entire energy consumed during the transportation is needed only for the food refrigeration, it is clear that refrigerated food transportation has to find novel solutions which ensure the quality and safety of the cargo and, contemporary, reduce the polluting emissions. For these reasons, researchers have started to make efforts in implementing LTES in the refrigerated transport field. Ahmed et al. [29] introduced copper tubes filled with paraffin-PCM (RT5 [30]) inside the insulation walls of truck trailers. They obtained an average reduction of 29% in the peak heat flux transferring into the inner room. Liu et al. [28] developed an on-vehicle LTES unit charged by a stationary refrigeration unit in depot during the night, which led to 86.4% cost savings through lower energy consumption, with remarkable reduction in greenhouse gas emissions and noise. Calati et al. [21] investigated the addition of a PCM layer (with thicknesses ranging from 0.5 to 2 cm) to the traditional 5 cm insulated PU wall and analyzed its ability in maintaining a proper air temperature inside the cell (empty of freight) by using three commercial paraffin waxes: RT2HC, RT4, RT5HC. The authors [21] considered the external solar irradiation by adopting the temperature sol-air model. They found that even the smallest thickness can potentially ensure the suitable condition for the entire 10 h simulated journey (from 6 AM to 4 PM), making the proposed solution to be a promising one. Ahn et al. [31] developed an innovative mobile cooling system which takes advantage of an ice thermal energy storage to cool down, with direct contact, the air during the discharging phase in a refrigerated truck. Liu et al. [32] developed a Phase Change Cold Storage Unit (PCCSU) to cool down the cold space at different refrigerated temperatures. The hot air circulates through the PCCSU being cooled down before being released in the refrigerated space. An energy cost reduction up to 91% compared with the solution without LTES system was calculated by the authors [32]

In this paper, aiming at extending the 2D numerical analyses conducted in Calati et al. [21] for the smallest thickness value (0.5 cm) and the lowest PCM melting temperature (2 °C), the presence of fresh foodstuffs is taken into consideration by adding 25%−50%−75% of cargo load in the refrigerated cell with respect to the total refrigerated vehicle. Different cargo typologies are investigated. The effect of the heat respiration of the freight is discussed aiming at evaluating the validity of the proposed passive system to ensure the safety of the foodstuff. Moreover, since the cooling performance can be altered by the pre-cooling level of the foodstuffs, three different cargo pre-cooling temperatures are studied (2 °C, 5 °C, 10 °C). The results are compared in terms of temperature evolution over time and temperature distribution inside the refrigerated cell.

2. Numerical analyses

2.1. The model

As reported in Calati et al. [21], a 2D section of a typical European refrigerated vehicle was modelled. Its external width ("top" and "bottom" in Fig. 1(a)) was set equal to 1.3 m (half of 2.6 m) aiming at exploiting the symmetry of the system, while its height was supposed to be 2.4 m ("side" in Fig. 1(a)). The problem is, in fact, axisymmetric with respect to an axis dividing the section in two identical zones (denoted as "symmetry" in Fig. 1(a)). Aiming at counteracting the heat load entering from the external environment, an innovative insulation layer was developed, having a 5 cm thick poly-urethane layer which wraps a second one of 0.5 cm filled of the commercial paraffin-based PCM

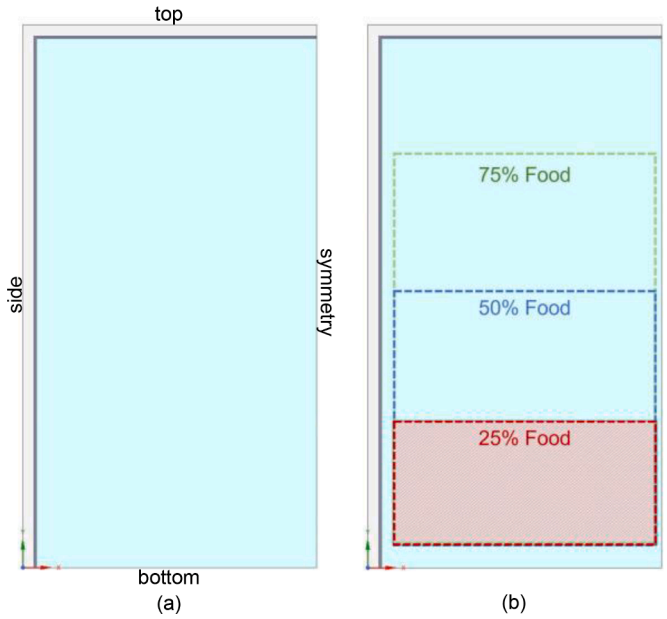

Fig. 1. 2D section of the refrigerated truck cell: empty (a), with food loads (b).

RT2HC supplied by Rubitherm [30], whose main properties are resumed in Table 1.

A thin aluminum layer of 0.5 cm acting as the PCM encapsulation to separate the PCM and the air domains is also added. For the sake of brevity, the entire description of the geometrical model will not be reported in the followings; the reader may refer to Calati et al. [21] for additional details.

In Fig. 1(b) the presence of the cold cargo that was considered in the present work can be appreciated. Different food loads were investigated, 25%−50%−75%. The smallest food load percentage represents the volume occupied by the foodstuffs during the final daily operation, 50% stands for an average value of the transported cargo, while 75% represents the almost full-loaded scenario, i.e., at the start of the truck daily operation. These different scenarios were compared among each other and with the empty scenario. The food cargo was modelled as a solid domain and consisted of, alternatively, three different materials (apple, broccoli, and tunafish) in order to investigate the effect of different food characteristics (see Table 2) on the thermal performance. Moreover, it is known that fresh foodstuffs (fruits and vegetables) are temperature-sensitive goods, and, having metabolic activity [33], they usually release the heat of respiration to the environment in which they are located [21]. The food was located 50 mm far from the walls and 20 mm from the axis of symmetry; two consecutive boxes are at a distance of 40 mm. Each box was supposed to have the x-dimension of 1170 mm and located on a 140 mm high europallet. The boxes were supposed to be positioned in this way so the generated buoyancy-driven airflow could flow under the pallets, in the space between the encapsulation and the cargo, and between the two cargoes. All the thermo-physical properties of the solid domains are shown in Table 2.

Table 1
Phase Change Material thermo-physical properties.

Melting range	1–3	°C
Solidification range	2–1	°C
Latent Heat, L	200	kJ kg^{-1}
Heat Capacity, c_p	2000	J kg^{-1}K^{-1}
Density (solid), ρ_{sol}	880	kg m^{-3}
Density (liquid), ρ_{liq}	770	kg m^{-3}
Heat Conductivity, k	0.2 (liquid and solid phases)	W m^{-1} K^{-1}
Volume Expansion	12.5	%
Flash Point	>100	°C
Max. Operation Temperature	40	°C

Table 2
Solid materials thermo-physical properties.

Material	k (W m^{-1}K^{-1})	ρ (kg m^{-3})	c_p (J kg^{-1}K^{-1})
Poly-Urethane foam	0.03	35	1380
Aluminum	202.4	2719	871
Apple	0.418	450	3840
Broccoli	0.385	560	4010
Tunafish	0.531	1070	3430

The presence of the external hourly solar irradiance was used to calculate the heat load entrance. By adopting the sol-air model [34] the fictitious free stream temperature *Tsa* was obtained as the sum of the external temperature and the ratio between the product of the solar irradiance for a tilted surface and the surface absorptance divided by the heat transfer coefficient *HTC*. For details, please refer to [21]. The *HTC* was set equal to 10 W m^{-2} K^{-1} for the side and top of the cell, whilst 0.7 W m^{-2} K^{-1} at the bottom which takes into consideration the non-modelled 5 cm poly-urethane foam layer. The appropriate *Tsa* was set for the side and top, which exchanged the heat by means of convection and radiation, whilst the external temperature was set as free stream temperature for the bottom, which, being in shadow, was not affected by solar radiation. The truck was supposed to be stationary aiming at investigating the worst-case scenario because the convective heat transfer due to the motion tends to decrease the wall temperature reducing the heat transferred to the cold chamber. This was demonstrated by Calati et al. [21] where the effects of the different truck speeds on the heat transfer were studied. Using the heat transfer coefficients calculated with the equation for flat plates [35], three different scenarios were investigated: stationary-scenario (0 km h^{-1} truck speed), urban-route-scenario (40 km h^{-1}) and interurban-route-scenario (80 km h^{-1}). The results showed that the stationary-scenario exhibited the highest sol-air temperatures for each truck surfaces. Therefore, this scenario was considered for the subsequent analyses. The boundary condition of the side of the truck involved the setting of the maximum hourly value of T_{sa} among the western and eastern ones for each simulated hour from 6 AM to 4 PM. The climate data refer to the city of Vicenza, Northern Italy. For all the scenarios (with or without food load) the temperature of the air in the refrigerated cell was initialized at 2 °C. The PCM, instead, was initialized at 0.5 °C in order to ensure its complete solid state before running the simulations. The food load was initialized at 2 °C, but, when investigating the pre-cooling temperature effect, it was set at an initial temperature of 5 °C or 10 °C.

2.2. Models

To estimate the global solar radiation for each truck surfaces, the same equations reported in [21] were adopted. For the sake of brevity, they are not explained here.

To study the thermal performance of the innovative proposed LTES system, the “Solidification and Melting Model” was adopted to run the CFD numerical simulation in the “Ansys Fluent 18.2″ environment [36]. The potentiality of this model consists of an enthalpy-porosity approximation of the zone where the phase change process takes place, denoted as mushy zone [36]. In this model, in fact, the melting front is not tracked directly, but it can be deduced by calculating volume-averaged variables. The liquid-solid mushy zone is supposed to be representative of a porous material whose porosity is set as the liquid fraction. This latter is a parameter which stands for the fraction of the cell volume in liquid state, calculated for all cells in the domain. Consequently, in the mushy zone, the liquid fraction can assume a value ranging between 0, i.e., when the PCM is completely solid, and 1, i.e., when the PCM is fully melted.

The model prescribes to solve the energy equation (Eq. (5)), written in terms of enthalpy (Eq. (1)), considered as the sum of sensible enthalpy (Eq. (2)) and latent heat of fusion (Eq. (3)), as demonstrated in the

following equations:

$$H = h + \Delta H \tag{1}$$

$$h = h_{ref} + \int_{T_{ref}}^{T} c_p dT \tag{2}$$

$$\Delta H = \varphi L \tag{3}$$

$$\varphi = \begin{cases} 0, \ if \ T < T_{solidus} \\ \dfrac{T - T_{solidus}}{T_{liquidus} - T_{solidus}}, \ if \ T_{solidus} < T < T_{liquidus} \\ 1, \ if \ T > T_{liquidus} \end{cases} \tag{4}$$

$$\frac{\partial}{\partial t}(\rho H) + \nabla \cdot (\rho \boldsymbol{v} H) = \nabla \cdot (k \nabla T) \tag{5}$$

The momentum conservation equation (Eq. (6)) for the mushy region is solved by adding a momentum sink $\boldsymbol{S}$ (Eq. (7)) in the Navier-Stokes equation, as:

$$\frac{\partial}{\partial t}(\rho \boldsymbol{v}) + \nabla(\rho \boldsymbol{v}\boldsymbol{v}) = -\nabla p + \mu \nabla^2 \boldsymbol{v} + \rho g \epsilon (T - T_{ref}) + \boldsymbol{S} \tag{6}$$

$$\boldsymbol{S} = \frac{(1-\varphi)^2}{\varepsilon + \varphi^3} A_{mush} \tag{7}$$

The buoyancy force with Boussinesq approximation and the above-mentioned momentum sink can be appreciated in the last right two terms of Eq. (6), respectively. In Eq. (7), ε is a constant equal to 10^{-3}, which avoids dividing by zero when liquid fraction φ is zero (PCM completely solid).

In order to analyze the food heat respiration effect on the thermal fluid dynamics, an energy source in the energy equation was added by treating the food domain as a heat source. A user-define-function (UDF) was developed to calculate the heat respiration as a function of the food temperature and implemented accordingly. The equation (Eq. (8)) of the heat of respiration of the food, HR (Wmm^{-3}), adapted from [37], considered in the present analyses is:

$$HR = \rho \frac{10.7f}{3600} \left(\frac{9}{5} t + 32 \right)^g \tag{8}$$

Where, t (°C) is the food temperature, ρ ($kg\ m^{-3}$) is the food density, f and g constant respiration coefficients which are specific for each fresh foodstuff (apples or broccoli) [37]. In particular, f values are $1.26 \cdot 10^{-6}$ and $4.86 \cdot 10^{-6}$, and g values are 2.5977 and 2.5728 for apples and broccoli, respectively.

Additionally, the conservation of mass is solved:

$$\nabla \cdot (\rho \boldsymbol{v}) = 0 \tag{9}$$

The convective terms with first order derivatives were linearized by adopting a second order upwind scheme, while a second order differencing scheme was preferred to linearize the diffusive terms with second order derivatives. The SIMPLE scheme was used to solve the pressure-velocity coupling while the PRESTO! one was chosen for pressure correction, as proposed by Zhao et al. [38]. All of the other equations were linearized using the algebraic multigrid (AMG) iterative strategy.

2.3. Model validation and sensitivity analyses

The present authors aimed at validating the proposed model of the novel LTES system by considering the experiments reported in [39]. The model proposed by [39] was developed and validated against experimental results, so, it was supposed to be a reliable case on which validating the model of this work. In particular, Glouannec et al. [39] considered two non-food-loaded scenarios. The first scenario (denoted by the present authors as "sensible-case") involved the construction of an airtight and insulated box, with one of the walls consisting of an 86 cm tall composite layer made of a thin metal sheet, a 10 cm air gap, a 5.8 cm thick polyurethane layer wrapped on the left and right faces by 0.1 cm of fiberglass and 0.2 cm of polyester and fiberglass, respectively. The internal temperature of the adiabatic box was fixed and maintained at 0 °C by a refrigeration system, while the temperature of the external environment was set at 10 °C for the first half of the test (4 h) and 30 °C for the second half (4 h). The second scenario (here denoted as "latent-case") regarded the insertion of a panel filled with Energain ®, which is a commercial phase change material [40], just before the fiber glass layer. In this last case, the external temperature was maintained at 10 °C for the first 8 h and 30 °C for the last 8 h The temperatures over time at different locations were monitored and collected. As already shown in [21], the numerical results coming from the here presented model are very close to the experimental results, with average percentage deviations less than 5% for both the sensible and latent cases, confirming the validity of the model.

As shown in Fig. 2, the mesh sensitivity analysis was run. The 25% food loaded refrigerated cell was selected as reference case, on which tuning the best grid constructive parameters. To compare the different results, the liquid fraction evolution curves over the 10 simulated hours were chosen. From Fig. 2 the independence of the solution from the grid can be appreciated. It is clear that the three different investigated meshes (26k, 50k, 99k elements) didn't take to different solutions, even if having different computational times to complete the simulation. Therefore, aiming at limiting as much as possible the computational errors, the 50k elements mesh was considered to be the best compromise and, the parameters chosen to generate the 50k elements mesh were selected and then adopted for the simulations of the other scenarios.

For what concerns the time step size, the value of 0.1 s was considered the best trade off between solution accuracy and computational efforts, thus selected and adopted even for the subsequent analyses. For additional details, the reader may refer to [21].

3. Results

In Fig. 3, the volume-averaged air temperature (Fig. 3(a)), PCM temperature (Fig. 3(b)), liquid fraction (Fig. 3(c)) and apple temperature (Fig. 3(d)) as function of the simulated hours for the empty and apple cargo loaded scenarios are shown. The capability of the LTES system in ensuring the air temperature inside the cell as close as possible to the reference phase change PCM temperature without involving the

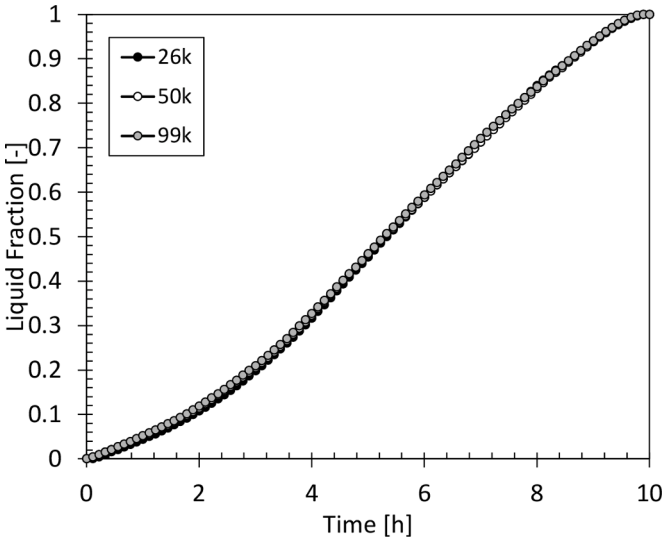

Fig. 2. Mesh sensitivity analysis for the 25% food loaded scenario.

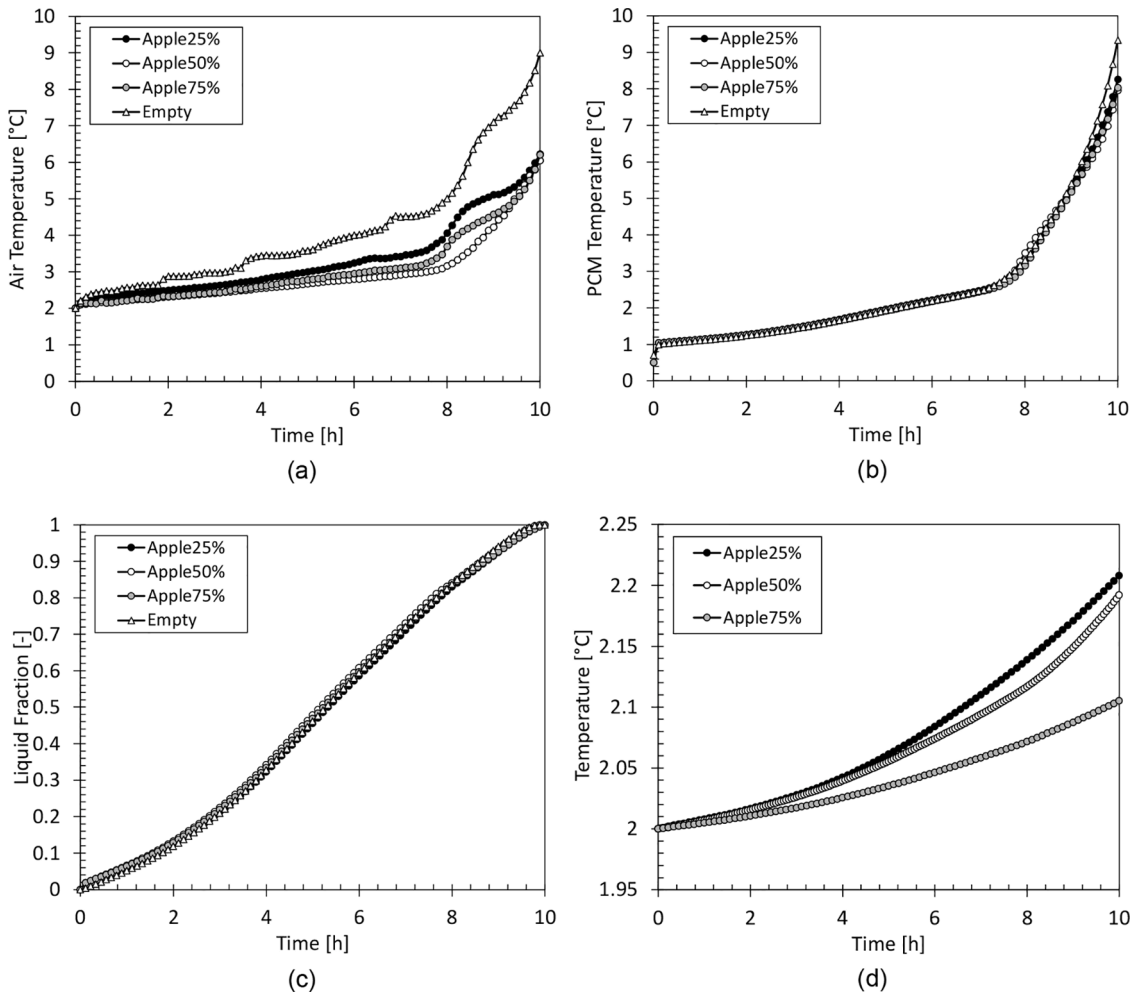

Fig. 3. Air temperature (a), PCM temperature (b), liquid fraction (c), apple temperature (d) curve evolutions, with different food loads.

adoption of the refrigerated system is investigated. By focusing on the empty scenario (white triangles) it can be noticed that the air temperature of the refrigerated cell is maintained below 3 °C for the first 4 h This threshold (3 °C) is the *liquidus* temperature of the PCM: therefore, when the temperature exceeds 3 °C the PCM is locally melted. For the subsequent 4 h, the air temperature is kept between 3 °C and 4 °C while, just after the eighth investigated hour, a sharp temperature increase can be seen. Indeed, from the ninth hour till the end of the simulated vehicle route, a noticeable change of slope for the air temperature can be observed. This behavior can be ascribable to the progress of the PCM melting process causing the ability of the paraffin in counteracting the external heat load penetration to be weakened, resulting in an air temperature increase. Additionally, in the period from the seventh and the eighth hour, a sudden average PCM temperature rise can be appreciated (Fig. 3(b)). The comparison between the PCM temperature curve with the liquid fraction one lets to point out that for the most part of the melting process (about 8 h, i. e. 85% liquid, Fig. 3(c)) the PCM temperature is maintained between the *solidus* and *liquidus* temperatures.

As a result, the capacity of the paraffin-based PCM layer in limiting the external heat to be transmitted inside the refrigerated cell is compromised since the PCM is almost completely melted. The sharp rise in the PCM temperature causes the air temperature to be increased, up to 9.5 °C; this is essentially caused by the sensible heat transfer due to the almost complete liquid PCM. It is well known that this value can potentially be detrimental for perishable goods which must be transported at temperatures around 2–3 °C.

Nevertheless, different air temperature evolutions can be detected when the cold freight is inserted inside the refrigerated cell. Focusing on Fig. 3(a) it can be immediately observed, that, despite the similar trends, significantly different final air temperature values are reached. As already stated, in the empty scenario the final air temperature reaches 9.5 °C. When the cold cargo is inside the refrigerated truck cell a final temperature of about 6 °C is calculated, which lets to maintain the perishable transported goods in an appropriate environment for the preservation of their quality and safety. By comparing the four air temperature curves in Fig. 3(a), it can be stated that all of them present a sharp temperature increase at the eighth hour, since the air temperature is strictly related to the PCM temperature evolution. Despite the diverse food loads, the PCM temperature curves (Fig. 3(b)) and liquid fraction curves (Fig. 3(c)) mostly overlap. This is due to the fact that the PCM temperature and the melting process, consequently, depend mostly on the external applied environmental conditions which are exactly the same for all the investigated scenarios. The presence of the different cold freight has a more evident impact on the air temperature inside the refrigerated cell (Fig. 3(a)) and, obviously, on the food temperature (Fig. 3(d)). By focusing on Fig. 3(a), the effect of the three apple load percentages on the air temperature evolutions can be detected. It is interested to notice that the lowermost temperature curve for each simulated instant is ensured by the 50% food loaded case, the 75% is set at an intermediate level while 25% leads to the highest temperatures. It is clear that all the food loaded investigated cases lead to an air temperature lower than the empty scenario throughout the journey. This phenomenon can be explained by comparing the air temperature distributions among the three food load scenarios and with the temperature

distribution inside the refrigerated cell for the empty case, as shown in Fig. 4.

Three instants are chosen to compare the different scenarios: the start of the route (6:00), the middle of the route (11:00) and the end of the route (16:00). By focusing on the empty cabin firstly, it can be observed that a main convective cell is formed in the middle of the refrigerated compartment. The convective movement is due to the air heated from the bottom which causes the air to be moved upwards. When reaching the top of the cabin, the air is cooled down by the PCM which is a at a lower temperature, as it can be noticed by comparing Fig. 3(a) and (b). The air circulation exists until a temperature gradient between the air and PCM remains sufficient. As a result, at the end of the simulation, when the temperature differences become negligeable, the air tends to stratify horizontally, reaching an average value around 9.5 °C. A similar behavior can be detected when a 25% apple load is put inside the cold cabin. A main convective cell is, in fact, generated during the journey while a horizontal temperature stratification is visualized at the final stage of the daily operation. Unlike the empty scenario, the final average air temperature is significantly lower, since the addition of the food load acts as a cold thermal mass which reduces the air temperature increase, even if the PCM is completely melted. Therefore, a final average temperature of 6 °C can be reached. A different temperature distribution can be identified for the 50% food loaded scenario. When considering the temperature contours at 11:00 (Fig. 4), the main convective cell cannot be observed anymore. There are only some local generated vortices since the presence of half of the volume occupied by the food cargo does not let the air to easily recirculate. When 75% of foodstuff is analyzed, local vortices cannot be clearly identified, since the low space available for the air movement. However, from what just stated and from what shown in Fig. 3(a), the 50% food loaded cabin always presents the lowest temperature at each instant since it can take advantage of the double concurrent effects of the air heat exchanged by convection and the presence of a significant additional thermal cold mass during the simulated route. The scenario involving the insertion of 50% food cargo can be therefore considered the best trade off. It can also be concluded that the cold food cargo load inside the proposed LTES system has a positive contribution in preserving and maintaining the optimal temperature distribution condition.

The same conclusions can be also found for the other two investigated food cargo materials: broccoli and tunafish.

As, in fact, reported in Fig. 5, broccoli (Fig. 5(a)) and tunafish (Fig. 5 (b)) present an air temperature curve evolution over time which is comparable with what obtained by adopting apples (Fig. 3). This suggests that our LTES system is a valid solution, independently from the transported cargo typology.

When dealing with temperature sensitive perishable foodstuffs, it is necessary to take into consideration the effect of their intrinsic metabolic activities since they can potentially negatively affect the maintenance of the suitable temperature condition. In the worst case, uncontrolled metabolic activities can take to food losses and wastages.

Therefore, the present authors investigated the effect of the heat of respiration, as reported in Eq. (8), by monitoring the air cabin temperature and the food temperature during the daily simulated route.

As shown in Fig. 6, the effect of the heat of respiration (denoted as "HR" in the legends) can be appreciated. By following the air temperature curves for the three food loaded studied scenarios, it can be observed that the heat of respiration does not have an evident impact on the air temperature. Consequently, for each food load the air temperature curves with or without the considered relative heat of respiration almost overlap. In fact, under the simplified assumptions set for the proposed LTES system (no heat infiltrations due to door openings and only 10 h daily route supposed) the heat of respiration seems to be negligeable since the temperature increase occurs at the final stages only. However, by focusing on Fig. 6(b) and by choosing, for example, the 50% food load case, it is evident the effect of the heat of respiration on the food temperature. At the tenth simulated hour, when the heat of respiration is not added to the numerical model, the temperature of the food reaches 2.17 °C, while it reaches about 2.38 °C under the effect of the heat of respiration. Moreover, the growing rate of the curve that considers the effect of the heat of respiration is sensibly higher than the

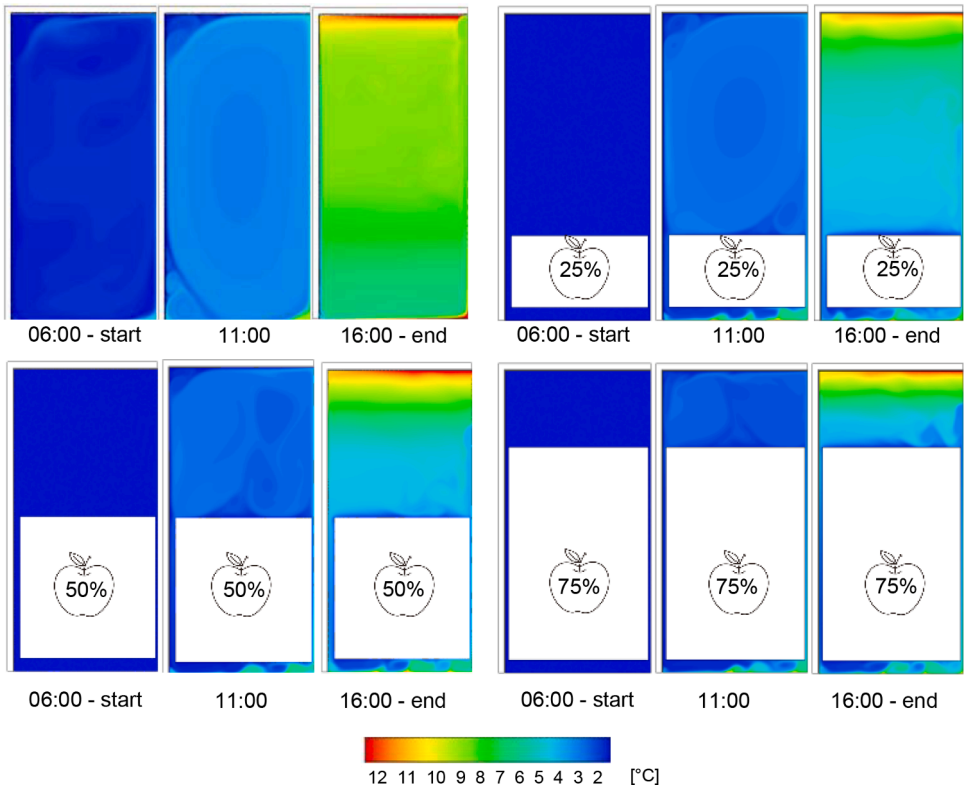

Fig. 4. Air temperature distribution inside the refrigerated cell, for the empty scenario and 25% −50% - 75% food load scenarios, at three different instants.

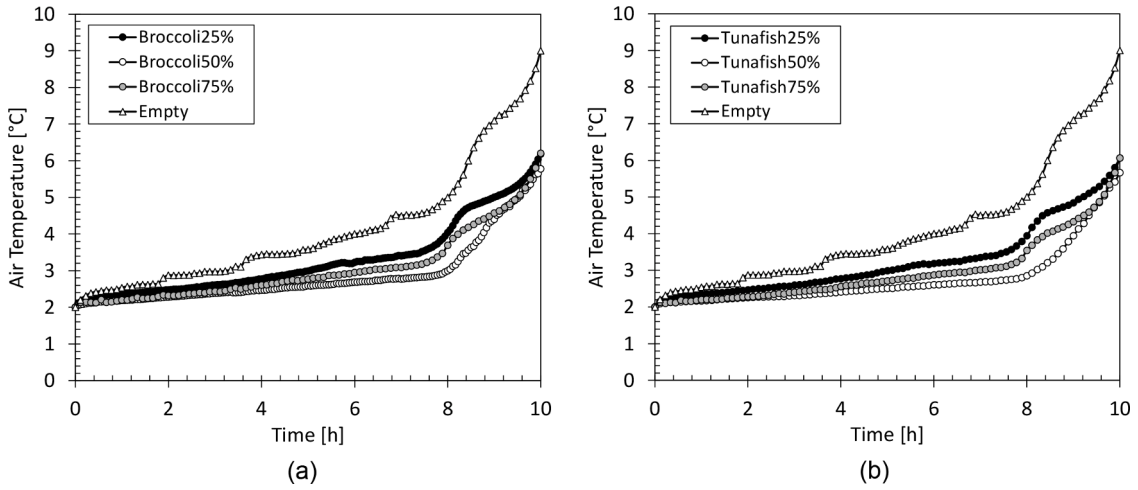

Fig. 5. Air temperature curve evolutions for different food loaded scenarios and materials: (a) broccoli, (b) tunafish.

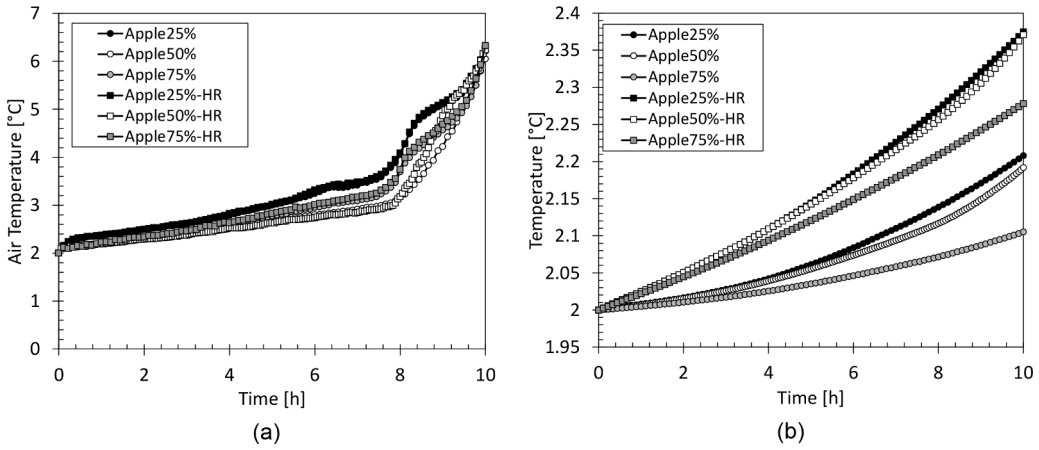

Fig. 6. Air (a) and food (b) temperature curve evolutions for different food loaded scenarios, with and without considering the effect of the heat of respiration.

one without it. Thus, it can be speculated, that, at the end of simulation, since the PCM is almost fully liquid, the role of the heat of respiration would be more important if an extension of the truck route is simulated.

Moreover, the fresh foodstuffs usually receive a pre-cooling process before entering the refrigerated truck [37]. It is not always necessary for the cargo to be cooled down to the temperature of the cold air (2 °C in the proposed solution). Therefore, by fixing a food load of 25%, the authors investigate the effect of the food precooling temperature. Three different values are chosen: 2 °C, 5 °C, and 10 °C. Additionally, for each pre-cooling level, the effect of the heat of respiration is also studied.

From what demonstrated in Fig. 7, it can be noticed that the pre-cooling food temperature has an impact on the thermal performance of the system. When the food enters at a temperature of 5 °C, the air, starting at 2 °C, needs about 8 h to reach that temperature, since the ability of the LTES in reducing the temperature increase. However, when the food is pre-cooled at 10 °C, the air jumps quickly to 5.5 °C and then reaches 8 °C in 7 h; the temperature of 8 °C can be considered the critical threshold at which the fresh product can be maintained in order to not lose the quality. Thus, the suitable conditions are ensured for 7 h only. Moreover, the higher the pre-cooling temperature, the higher the heat of respiration effect. In fact, the heat of respiration let the final temperature to be 0.3 °C, 0.65 °C, 1.08 °C higher than the one without the heat of respiration, for 2 °C, 5 °C, and 10 °C, respectively. Besides, from the simulations, when the heat of respiration is not considered, it is found that the food temperature remains almost constant during the route, facing a very low temperature decrease: when the food is inserted at

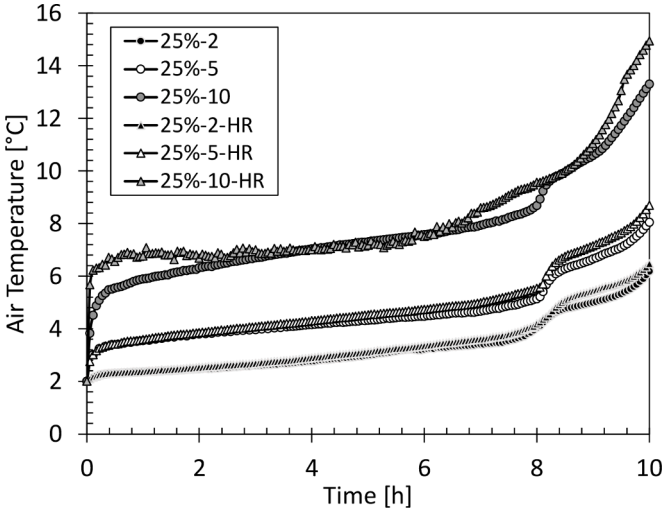

Fig. 7. Air temperature evolution for the 25% food load and different pre-cooling temperature (2 °C, 5 °C, 10 °C) with or without heat of respiration.

10 °C it reaches 9.6 °C at the end of simulation, while when entering at 5 °C, it reaches 4.9 °C. This suggests that for the proposed LTES system, the determination of the appropriate pre-cooling temperature is

essential. In fact, the system is not able to cool down the food, but, only able to mitigate its temperature sudden rise. Moreover, it is interesting to compare the food and air temperature increase at different food loads and different pre-cooling levels.

In Fig. 8 the temperature increase $\Delta T_{f\text{-}o}$, defined as the difference between the final temperature T_f and the initial temperature T_o, for the air and food cargo, against the pre-cooling temperature T_{in} is plotted. It is clear that, when the cargo is put inside the truck at a temperature level equal to the air cell (2 °C) the food experiences a very low temperature increase (almost 0.3 °C) for each food load values, even if the effect of the heat of respiration is taken into consideration. In fact, the cold mass mitigates the temperature increase. Even the air temperature increase for the three food loads is very similar, being limited at about 4.2 °C. A different behavior happens when T_{in} is equal to 5 °C. In this scenario, the food temperature increases of some of 1 °C for the 25%, 50% and 75% food load cases. Being the heat of respiration function of the food temperature, as stated above, the higher the food temperature, the higher the HR effect. It is evident that the higher the food load, the higher the air temperature increase. The 75% food load scenario presents a ΔT of about 8 °C, meaning that the final temperature has approached 10 °C, which can be a dangerous level for fresh foodstuffs. A more remarkable temperature increase rate can be observed when the cargo is pre-cooled at 10 °C. In this case, in fact, even if relative low temperature increases are reported for the food (an average increase of 1.5 °C), the final food temperature is over 11 °C. Besides, the air temperatures suffer of considerable temperature increasing (with a maximum of 14 °C for the 75% food load scenario) since the higher contribution of the heat of respiration due to the food higher temperatures. This suggests that our proposed system, being fully passive, is not able to cool down the cargo. As a consequence, the food, remains at a dangerous level for the entire route.

Therefore, for a further development of the LTES system for refrigerated truck, it may be necessary to consider the insertion of a small active refrigeration unit needed for the immediate cooling of the foodstuff only. Then, after having reached the desired temperature, the active system may be switched off and the temperature of the system would be maintained at an appropriate level due to the action of the LTES.

4. Conclusion

In this work, the thermal performance of an innovative LTES system for a refrigerated truck is studied. The system consists of a novel insulation layer made by a 5 cm traditional PU-foam layer wrapping a 0.5 cm PCM layer. The ability of the system in counteracting the external heat load gain with a cabin temperature starting at 2 °C is investigated. Four different scenarios are analyzed: an empty one, and three food loaded cases (25%, 50%, 75% food loaded) representing three different moments of a traditional daily route. It is obtained that, the 50% cargo loaded scenario lets to reach the lowest air temperature inside the refrigerated compartment during the 10 h, since it exploits the double concurrent effect of the air heat exchanged by natural convection and the presence of a significant additional thermal cold mass. Moreover, being this system proposed for temperature-sensitive cargoes, the role of the heat of respiration due to metabolic activities is analyzed. It is found that it has a more impactful role during the final instants of the route when the PCM is almost completely liquid and, so, not able to counteract the heat entrance. Additionaly, the pre-cooling temperature level is demonstrated to have a significant impact on ensuring the suitable temperature conditions of the LTES system. In fact, when the cargo is inserted at 5 °C, only the 25% food load scenario ensures the final temperature to be contained into a safe level. 75% of food entering at 5 °C lets the air cell to reach a final temperature of about 10 °C. The proposed system cannot control or cool down the food because it is only meant to maintain the safe conditions for the entire route. In order to handle different pre-cooling cargoes, a different active solution needs to be considered and adopted, but this does not limit the promising capabilities of the proposed technology in reducing the GHG emissions and the energy costs.

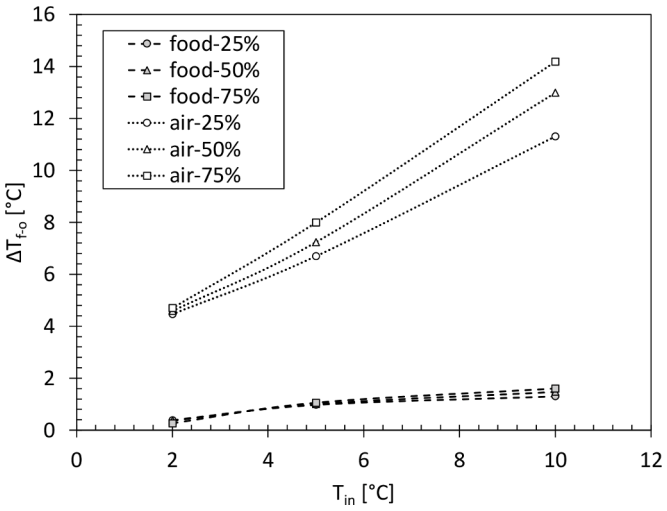

Fig. 8. Air and food temperature increase for different food loads (25%- 50%-75%) and different pre-cooling levels (2 °C, 5 °C and 10 °C).

Declaration of Competing Interest

The authors declare that they have no known competing financial interests or personal relationships that could have appeared to influence the work reported in this paper.

Data availability

No data was used for the research described in the article.

Acknowledgment

The authors wish to acknowledge the support and the computational resources made available by the High Performance Computing Lab at the Department of Management and Engineering (DTG), co-funded by the University of Padova in the framework of the program "Scientific research instrumentation 2015".

References

[1] UN-environment programme, "Sustainable cold chain and food loss reduction," 2019. Accessed: Jun. 03, 2022. [Online]. Available: https://ozone.unep.org/system/files/documents/MOP31-Sustainable-HL_Briefing_Note.pdf.

[2] J. Gustavsson, Food and agriculture organization of the United Nations., and N. ASME/Pacific rim technical conference and exhibition on integration and packaging of MEMS, in: Proceedings of the Global Food Losses and Food Waste: Extent, Causes and Prevention: Study Conducted for the International Congress "Save Food!" at Interpack 2011 Düsseldorf, 2022. Germany. Accessed: Jun. 03 [Online]. Available, https://www.fao.org/3/mb060e/mb060e00.htm.

[3] Food and Agriculture Organization of the United Nations and Food Wastage Footprint (Project), *Food wastage footprint full-cost accounting: final report.* Accessed: Jun. 03, 2022. [Online]. Available: https://www.fao.org/3/i3991e/i3991e.pdf.

[4] IIR_UN Environment, "Cold chain technology brief: transport refrigeration," 2018. Accessed: Jun. 03, 2022. [Online]. Available: https://wedocs.unep.org/bitstream/handle/20.500.11822/32571/8142Transpor_Ref_EN.pdf?sequence=1&isAllowed=y.

[5] Food and Agriculture Organization of the United Nations, International fund for agricultural development, UNICEF, world food programme, and world health organization, *the state of food security and nutrition in the world : safeguarding against economic slowdowns and downturns.* Accessed: Jun. 03, 2022. [Online]. Available: https://www.fao.org/3/ca5162en/ca5162en.pdf.

[6] J.A. Evans, E.C. Hammond, A.J. Gigiel, L. Reinholdt, K. Fikiin, C. Zilio, Assessment of methods to reduce the energy consumption of food cold stores, Appl. Therm. Eng. 62 (2) (2014) 697–705, https://doi.org/10.1016/j.applthermaleng.2013.10.023.

[7] EASE, "Thermal storage position paper," 2017.
[8] S.A. Tassou, J.S. Lewis, Y.T. Ge, A. Hadawey, I. Chaer, A review of emerging technologies for food refrigeration applications, Appl. Therm. Eng. 30 (4) (2010) 263–276, https://doi.org/10.1016/j.applthermaleng.2009.09.001. Mar.
[9] M. Mirmanto, S. Syahrul, Y. Wirdan, Experimental performances of a thermoelectric cooler box with thermoelectric position variations, Eng. Sci. Technol. Int. J. 22 (1) (2019) 177–184, https://doi.org/10.1016/j.jestch.2018.09.006. Feb.
[10] A. Çağlar, Optimization of operational conditions for a thermoelectric refrigerator and its performance analysis at optimum conditions, Int. J. Refrig. 96 (2018) 70–77, https://doi.org/10.1016/j.ijrefrig.2018.09.014. Dec.
[11] E. Söylemez, E. Alpman, A. Onat, S. Hartomacıoğlu, CFD analysis for predicting cooling time of a domestic refrigerator with thermoelectric cooling system, Int. J. Refrig. 123 (2021) 138–149, https://doi.org/10.1016/j.ijrefrig.2020.11.012. Mar.
[12] X.H. Yuan, C.H. Qin, Y.P. Wang, X. Liu, Characteristics analysis of small insulated vans based on thermoelectric cooling, Front. Energy Res. 9 (2021), https://doi.org/10.3389/fenrg.2021.740748. Sep.
[13] S.A. T.assou, G. De-Lille, Y.T. G.e, Food transport refrigeration - approaches to reduce energy consumption and environmental impacts of road transport, Appl. Therm. Eng. 29 (8–9) (2009) 1467–1477, https://doi.org/10.1016/j.applthermaleng.2008.06.027. Jun.
[14] E. Douvi, et al., Phase change materials in solar domestic hot water systems: a review, Int. J. Thermofluids 10 (2021), https://doi.org/10.1016/j.ijft.2021.100075. Elsevier B.V., May 01.
[15] G. Dogkas, et al., Investigating the performance of a thermal energy storage unit with paraffin as phase change material, targeting buildings' cooling needs: an experimental approach, Int. J. Thermofluids 3–4 (2020), https://doi.org/10.1016/j.ijft.2020.100027. May.
[16] B. Alshuraiaan, Efficient utilization of PCM in building envelope in a hot environment condition, Int. J. Thermofluids 16 (2022), https://doi.org/10.1016/j.ijft.2022.100205. Nov.
[17] G. Righetti, L. Doretti, C. Zilio, G.A. Longo, S. Mancin, Experimental investigation of phase change of medium/high temperature paraffin wax embedded in 3D periodic structure, Int. J. Thermofluids 5–6 (2020), https://doi.org/10.1016/j.ijft.2020.100035. Aug.
[18] M.A. Ezan, E. Ozcan Doganay, F.E. Yavuz, I.H. Tavman, A numerical study on the usage of phase change material (PCM) to prolong compressor off period in a beverage cooler, Energy Convers. Manag. 142 (2017) 95–106, https://doi.org/10.1016/j.enconman.2017.03.032.
[19] W. Lu, S.A. Tassou, Characterization and experimental investigation of phase change materials for chilled food refrigerated cabinet applications, Appl. Energy 112 (2013) 1376–1382, https://doi.org/10.1016/j.apenergy.2013.01.071.
[20] "https://www.vikingcold.com/." https://www.vikingcold.com/ (accessed Jun. 03, 2022).
[21] M. Calati, C. Zilio, G. Righetti, G.A. Longo, K. Hooman, S. Mancin, Latent thermal energy storage for refrigerated trucks, Int. J. Refrig. 136 (2022) 124–133, https://doi.org/10.1016/j.ijrefrig.2022.01.018. Apr.
[22] H. Jouhara, A. Żabnieńska-Góra, N. Khordehgah, D. Ahmad, T. Lipinski, Latent thermal energy storage technologies and applications: a review, Int. J. Thermofluids 5–6 (2020), https://doi.org/10.1016/j.ijft.2020.100039. Aug.
[23] C. Pagkalos, G. Dogkas, M.K. Koukou, J. Konstantaras, K. Lymperis, M. G. Vrachopoulos, Evaluation of water and paraffin PCM as storage media for use in thermal energy storage applications: a numerical approach, Int. J. Thermofluids 1–2 (2020), https://doi.org/10.1016/j.ijft.2019.100006. Feb.
[24] O. Okogeri, V.N. Stathopoulos, What about greener phase change materials? A review on biobased phase change materials for thermal energy storage applications, Int. J. Thermofluids 10 (2021), https://doi.org/10.1016/j.ijft.2021.100081. Elsevier B.V., May 01.
[25] A. Sharma, V.V. Tyagi, C.R. Chen, D. Buddhi, Review on thermal energy storage with phase change materials and applications, Renew. Sustain. Energy Rev. 13 (2) (2009) 318–345, https://doi.org/10.1016/j.rser.2007.10.005.
[26] H. Selvnes, Y. Allouche, R.I. Manescu, A. Hafner, Review on cold thermal energy storage applied to refrigeration systems using phase change materials, Therm. Sci. Eng. Prog. 22 (2021), https://doi.org/10.1016/j.tsep.2020.100807. Elsevier Ltd, May 01.
[27] M. Calati, K. Hooman, S. Mancin, Thermal storage based on phase change materials (PCMs) for refrigerated transport and distribution applications along the cold chain: a review, Int. J. Thermofluids 16 (2022), 100224, https://doi.org/10.1016/j.ijft.2022.100224.
[28] M. Liu, W. Saman, F. Bruno, Development of a novel refrigeration system for refrigerated trucks incorporating phase change material, Appl. Energy 92 (2012) 336–342, https://doi.org/10.1016/j.apenergy.2011.10.015.
[29] M. Ahmed, O. Meade, M.A. Medina, Reducing heat transfer across the insulated walls of refrigerated truck trailers by the application of phase change materials, Energy Convers. Manag. 51 (3) (2010) 383–392, https://doi.org/10.1016/j.enconman.2009.09.003. Mar.
[30] "Rubitherm, DE." https://www.rubitherm.eu (accessed Sep. 27, 2022).
[31] J.H. Ahn, H. Kim, Y. Jeon, K.H. Kwon, Performance characteristics of mobile cooling system utilizing ice thermal energy storage with direct contact discharging for a refrigerated truck, Appl. Energy 308 (2022), https://doi.org/10.1016/j.apenergy.2021.118373.
[32] G. Liu, et al., Improving system performance of the refrigeration unit using phase change material (PCM) for transport refrigerated vehicles: an experimental investigation in South China, J. Energy Storage 51 (2022), https://doi.org/10.1016/j.est.2022.104435.
[33] R. Fioretti, P. Principi, B. Copertaro, A refrigerated container envelope with a PCM (Phase Change Material) layer: experimental and theoretical investigation in a representative town in Central Italy, Energy Convers. Manag. 122 (2016) 131–141, https://doi.org/10.1016/j.enconman.2016.05.071.
[34] M. Calati, L. Doretti, C. Zilio, S. Mancin, 3D numerical simulation of a novel ventilated roof: thermal performance analysis and fluid flow behavior, Sci. Technol. Built. Environ. 27 (6) (2021) 819–831, https://doi.org/10.1080/23744731.2021.1917931.
[35] F.P. Incropera, D.P. Dewitt, T.L. Bergman, and A.S. Lavine, *Fundamentals of Heat and Mass Transfer*. 2007.
[36] "Ansys Fluent Manual." (2023) https://www.afs.enea.it/project/neptunius/docs/fluent/html/ug/main_pre.htm.
[37] American Society of Heating Refrigerating and Air-Conditioning Engineers., 2018 *ASHRAE handbook : refrigeration*.
[38] C. Zhao, et al., Simulations of melting performance enhancement for a PCM embedded in metal periodic structures, Int. J. Heat Mass Transf. 168 (2021), https://doi.org/10.1016/j.ijheatmasstransfer.2020.120853. Apr.
[39] P. Glouannec, B. Michel, G. Delamarre, Y. Grohens, Experimental and numerical study of heat transfer across insulation wall of a refrigerated integral panel van, Appl. Therm. Eng. 73 (1) (2014) 196–204, https://doi.org/10.1016/j.applthermaleng.2014.07.044. Dec.
[40] "-." (2023) http://buildinginnovations.dupont.com/en_GB_energain_contact.